Available online at www.sciencedirect.com
SCIENCE DIRECT®
Advances in Water Resources 29 (2006) 471–480
Advances in Water Resources
www.elsevier.com/locate/advwatres

New analytical solutions for groundwater flow in wedge-shaped aquifers with various topographic boundary conditions

Hund-Der Yeh *, Ya-Chi Chang

Institute of Environmental Engineering, National Chiao Tung University, 75 Po-Ai Street, Hsinchu 30039, Taiwan

Received 24 March 2005; accepted 16 June 2005
Available online 2 August 2005

Abstract

The hydraulic head distribution in a wedge-shaped aquifer depends on the wedge angle and the topographic and hydrogeological boundary conditions. In addition, an equation in terms of the radial distance with trigonometric functions along the boundary may be suitable to describe the water level configuration for a valley flank with a gentle sloping and rolling topography. This paper develops a general mathematical model including the governing equation and a variety of boundary conditions for the groundwater flow within a wedge-shaped aquifer. Based on the model, a new closed-form solution for transient flow in the wedge-shaped aquifer is derived via the finite sine transform and Hankel transform. In addition, a numerical approach, including the roots search scheme, the Gaussian quadrature, and Shanks' method, is proposed for efficiently evaluating the infinite series and the infinite integral presented in the solution. This solution may be used to describe the head distribution for wedges that image theory is inapplicable, and to explore the effects of the recharge from various topographic boundaries on the groundwater flow system within a wedge-shaped aquifer.

Keywords: Analytical solution; Finite sine transform; Hankel transform; Groundwater; Numerical approach; Wedge-shaped aquifer

1. Introduction

Theis [13] developed a solution for evaluating drawdown during pumping test analysis in a homogeneous, isotropic and non-leaky aquifer of infinite extent. However, the well-hydraulic theory cannot cope with the aquifers with impervious faults as no-flow boundaries or rivers as constant-head boundaries. In general, the solution for the hydraulic head distribution in a wedge-shaped aquifer with various boundaries may be obtained by adding imaginary wells known as the image wells. However, the image theory is applicable only when the angle between the bounding radii expressed as π/n where n is an integer [11]. Chan et al. [4] developed an analytic solution for drawdowns in rectangular aquifers. For the wedge-shaped aquifer, Chan et al. [5] applied the finite sine transform and Hankel transform to obtain the transient-state and steady-state drawdown solutions with an infinite wedge, and applied the finite sine transform and Mellin transform to obtain a steady-state drawdown solution which does not contain an infinite series term and is much easier to compute. Chan et al. [5] only considered the case of a zero-drawdown boundary, i.e., assuming the surface topography along the boundary is flat. Kuo et al. [8] utilized the image-well method to predict the drawdown distribution in aquifers with irregularly shaped boundaries; however, their solutions may diverge if insufficient number and improper locations of the image wells are employed.

Consider a non-leaky aquifer whose plan view is a sector of a circle. The groundwater flow in a wedge-shaped aquifer is analyzed in the polar coordinate system. Physically, a groundwater flow system with a

* Corresponding author. Tel.: +886 3 5731910; fax: +886 3 5726050.
E-mail address: hdyeh@mail.nctu.edu.tw (H.-D. Yeh).

0309-1708/$ - see front matter © 2005 Elsevier Ltd. All rights reserved.
doi:10.1016/j.advwatres.2005.06.002

wedge-shaped aquifer is commonly formed by ancient alluvial fan. The hydraulic head distribution within the sector naturally depends on the wedge angle and boundary conditions. The constant-head and no-flow boundary conditions are often used to represent the real-world hydrogeological boundary conditions. An annual average water level for a stream may be used as the boundary of time-independent head for a regional groundwater flow system if the bottom of the stream is connected with the aquifer. For a valley flank with a gentle sloping and rolling topography, an equation in terms of the trigonometric functions of radial distance along the boundary may be suitable to describe the water level configuration [14]. The purpose of this paper is to develop a general mathematical model with a variety of topographic and hydrogeological boundary conditions to describe the groundwater flow system in a wedge-shaped aquifer. In addition, the transient-state and steady-state solutions are derived based on the mathematical model and simplified to concise forms for easy computing. Furthermore, new mathematical formulas for Bessel functions are established in the derivation. These solutions contain integral from zero to infinity with an integrand comprising of a trigonometric function for the steady-state solution and a Bessel function for the transient-state solution. The integrals are difficult to accurately evaluate because of the oscillatory nature and slow convergence of the integrand. Therefore, a numerical approach, including the roots search scheme, the Gaussian quadrature, and Shanks' method, is proposed to evaluating the solution. These solutions seem to be difficult to evaluate, however, the proposed numerical approach can evaluate the solutions accurately and quickly. Several case studies are demonstrated in this paper and those cases may be considered as the applications of the solutions.

These new solutions are useful and valuable to analyze the groundwater flow in the wedge-shaped aquifer. These solutions can be used: (1) to describe the groundwater flow in a wedge-shaped aquifer under a variety of topographic and hydrogeological boundary conditions, (2) to predict drawdown for any wedge angle of the aquifer that the traditional method of image is not applicable, (3) to evaluate the sensitivity of the parameters in the mathematical model, and (4) to identify the hydraulic parameters when coupling with an optimization approach in aquifer data analysis.

2. Mathematical model

2.1. Governing equation and related boundary and initial conditions

Fig. 1 shows a wedge-shaped aquifer with an angle of ϕ and the boundaries of time-independent heads $p(r)$ and $q(r)$. These equations $p(r)$ and $q(r)$ represent the lower and upper boundaries with various topographic conditions, respectively. For a pumping well located at the point (r_0, θ_0) with a pumping rate Q, the differential equation governing the hydraulic head h at any point (r, θ) may be expressed as [5]

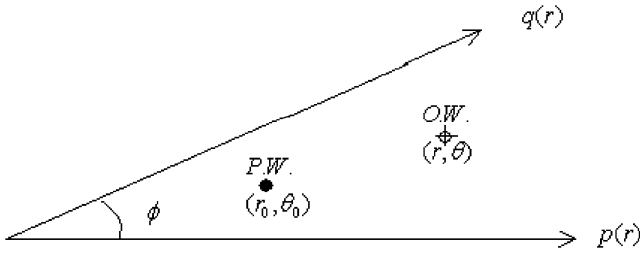

Fig. 1. The infinite wedge with boundary of time-independent head.

$$T\left(\frac{\partial^2 h}{\partial r^2}+\frac{1}{r}\frac{\partial h}{\partial r}+\frac{1}{r^2}\frac{\partial^2 h}{\partial \theta^2}\right)-S\frac{\partial h}{\partial t} = -\frac{Q}{r}\delta(r-r_0)\delta(\theta-\theta_0) \quad (1)$$

where T is the transmissivity (L^2/T); S is the storage coefficient; h is the hydraulic head (L); t is time from the start of the pumping test (T); r is the radial distance from the origin (L); and θ is the angle (radians) from the lower boundary. Fig. 2 shows the hydraulic head $h(r, \theta)$ along the boundary of time-independent head (e.g. a stream or a river) consisting of three components: h_0, h_1 and h_2 for representing a gentle sloping and rolling configuration where h_0 is a constant denoting the depth from the bottom of the aquifer. In addition, $h_1 = r\tan\alpha$ where α is the average slope of the boundary and h_2 may be approximated by [14]

$$h_2 = a\frac{\sin(br/\cos\alpha)}{\cos\alpha} \quad (2)$$

where a is the amplitude of the sine curve, $b = 2\pi/\lambda$ is the frequency, and λ is the period of the sine wave. Upon introducing the abbreviations $\tan\alpha = c'$, $a/\cos\alpha = a'$ and $b/\cos\alpha = b'$, the equations representing the hydraulic head of the lower and upper boundaries illustrated in Fig. 1 may be respectively written as:

$$h(r,\theta) = p(r) = h_p + c_1' r + a_1' \sin(b_1' r), \quad \theta = 0, \quad 0 \leqslant r \leqslant \infty \quad (3)$$

and

$$h(r,\theta) = q(r) = h_q + c_2' r + a_2' \sin(b_2' r), \quad \theta = \phi, \quad 0 \leqslant r \leqslant \infty \quad (4)$$

where h_p and h_q are the depth to the impervious strata for the lower and upper boundaries at the origin of the wedge-shaped aquifer, respectively. Also, the subscripts 1 and 2 denote the lower and upper boundaries respectively. In reality, h_p is generally equal to h_q;

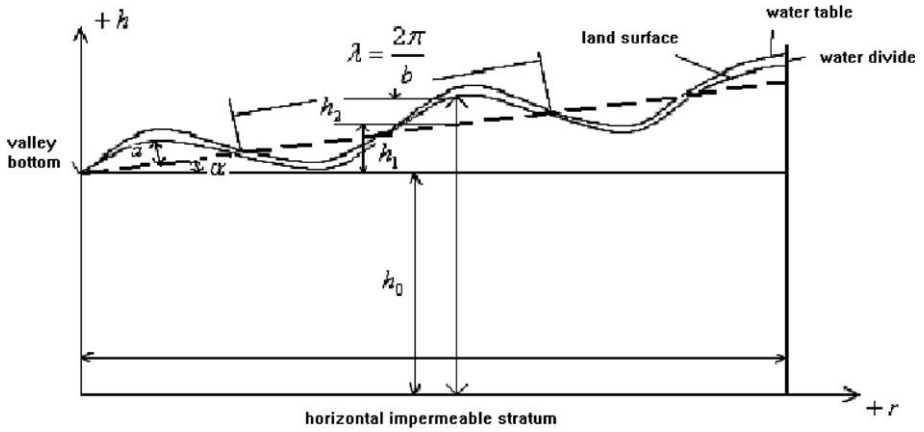

Fig. 2. Idealized cross-section of a valley flank in a small drainage basin.

however, h_p and h_q may not be the same if there is a fault located at the origin of the wedge-shaped aquifer. The initial condition, shown in Appendix A, is assumed as the solution of solving (1) when omitting $\partial h/\partial t$ and setting the pumping rate Q to be zero and with the boundary conditions of (3) and (4).

2.2. Analytical solutions for transient-state and steady-state problems

Since the governing equation, the initial condition and boundary conditions are specified, the solution of hydraulic head in a wedge-shaped aquifer with an infinite radius can be obtained via the finite sine transform and Hankel transform for (1)–(4). Detailed derivations for transient-state and steady-state solutions are given in Appendix A and the results are

$$h(r,\theta,t) = \frac{2}{\phi}\sum_{n=1}^{\infty}\sin(\mu_n\theta)\left[\frac{Q}{T}\sin(\mu_n\theta_0)(\Omega_1+\Omega_2) + \mu_n(c_1' - (-1)^n c_2')\Omega_3 + \mu_n(a_1'\Omega_4 - (-1)^n a_2'\Omega_5) + \mu_n(h_p - (-1)^n h_q)\Omega_6\right] \quad (5)$$

and

$$h(r,\theta) = \frac{2}{\phi}\sum_{n=1}^{\infty}\sin(\mu_n\theta)\left[\frac{Q}{T}\sin(\mu_n\theta_0)\Omega_2 + \mu_n(c_1' - (-1)^n c_2')\Omega_3 + \mu_n(a_1'\Omega_4 - (-1)^n a_2'\Omega_5) + \mu_n(h_p - (-1)^n h_q)\Omega_6\right] \quad (6)$$

with

$$\Omega_1 = \int_0^{\infty}\left[-\exp\left(\frac{-u^2 T}{S}t\right)\right]J_{\mu_n}(ur_0)J_{\mu_n}(ur)\frac{\mathrm{d}u}{u} \quad (7)$$

$$\Omega_2 = \int_0^{\infty} J_{\mu_n}(ur_0)J_{\mu_n}(ur)\frac{\mathrm{d}u}{u} \quad (8)$$

$$\Omega_3 = \int_0^{\infty}\frac{J_{\mu_n}(ur)}{u}\int_0^{\infty} J_{\mu_n}(u\kappa)\,\mathrm{d}\kappa\,\mathrm{d}u \quad (9)$$

$$\Omega_4 = \int_0^{\infty}\frac{J_{\mu_n}(ur)}{u}\int_0^{\infty}\sin(b_1'\kappa)\frac{J_{\mu_n}(u\kappa)}{\kappa}\,\mathrm{d}\kappa\,\mathrm{d}u \quad (10)$$

$$\Omega_5 = \int_0^{\infty}\frac{J_{\mu_n}(ur)}{u}\int_0^{\infty}\sin(b_2'\kappa)\frac{J_{\mu_n}(u\kappa)}{\kappa}\,\mathrm{d}\kappa\,\mathrm{d}u \quad (11)$$

$$\Omega_6 = \int_0^{\infty}\frac{J_{\mu_n}(ur)}{u}\int_0^{\infty}\frac{J_{\mu_n}(u\kappa)}{\kappa}\,\mathrm{d}\kappa\,\mathrm{d}u \quad (12)$$

and

$$\mu_n = \frac{n\pi}{\phi} \quad (13)$$

where u and κ are the dummy variables, and $J_{\mu_n}(\cdot)$ is the Bessel function of the first kind with order μ_n. The first and second terms (contain Ω_1 and Ω_2 respectively) on the right-hand side (RHS) of (5) represent the drawdown due to pumping, and the other terms represent the hydraulic head arisen from the slopes, curves, and elevations of the boundaries of the wedge-shaped aquifer respectively.

Notice that the presence of the Bessel functions of high order and large argument in (5) and (6) may be difficult to evaluate. Thus (5) and (6) are further simplified. The procedures of simplifications are presented in Appendix B, and the obtained transient-state and steady-state solutions can be respectively written as

$$h(r,\theta,t) = \frac{2}{\phi}\sum_{n=1}^{\infty}\sin(\mu_n\theta)\left[\frac{Q}{T}\sin(\mu_n\theta_0)\Omega_1\right] + \frac{Q}{4\pi T}(\log\gamma_1 - \log\gamma_2) + \frac{r}{\sin\phi}\{c_1'\sin(\phi-\theta) + c_2'\sin(\theta)\} + \varphi\left[a_1'\Lambda_1 + a_2'\Lambda_2\right] + \left[\frac{\theta}{\phi}(h_q - h_p) + h_p\right] \quad (14)$$

and

$$h(r,\theta) = \frac{Q}{4\pi T}(\log\gamma_1 - \log\gamma_2) + \frac{r}{\sin\phi}\{c_1'\sin(\phi-\theta) + c_2'\sin(\theta)\} + \varphi[a_1'\Lambda_1 + a_2'\Lambda_2] + \left[\frac{\theta}{\phi}(h_q - h_p) + h_p\right] \quad (15)$$

with

$$\Lambda_1 = \int_0^\infty \frac{u^{(\pi/\phi)-1}\sin(b_1'u)}{\psi_1}\,du \quad (16)$$

$$\Lambda_2 = \int_0^\infty \frac{u^{(\pi/\phi)-1}\sin(b_2'u)}{\psi_2}\,du \quad (17)$$

$$\psi_1 = u^{2\pi/\phi} - 2r^{\pi/\phi}u^{\pi/\phi}\cos\left(\frac{\pi}{\phi}\theta\right) + r^{2\pi/\phi} \quad (18)$$

$$\psi_2 = u^{2\pi/\phi} + 2r^{\pi/\phi}u^{\pi/\phi}\cos\left(\frac{\pi}{\phi}\theta\right) + r^{2\pi/\phi} \quad (19)$$

$$\varphi = \frac{r^{\pi/\phi}\sin\left(\frac{\pi}{\phi}\theta\right)}{\phi} \quad (20)$$

$$\gamma_1 = 1 - 2\left(\frac{r}{r_0}\right)^{\pi/\phi}\cos\frac{\pi(\theta+\theta_0)}{\phi} + \left(\frac{r}{r_0}\right)^{2\pi/\phi} \quad (21)$$

and

$$\gamma_2 = 1 - 2\left(\frac{r}{r_0}\right)^{\pi/\phi}\cos\frac{\pi(\theta-\theta_0)}{\phi} + \left(\frac{r}{r_0}\right)^{2\pi/\phi} \quad (22)$$

If $r > r_0$, the solution can be obtained by interchanging r and r_0 in both (21) and (22). Like the term in (5), the first and second terms on the right-hand side (RHS) of (14) represent the drawdown due to pumping, and the other terms represents the hydraulic head arisen from the slopes, curves and elevations of the boundaries of the wedge-shaped aquifer respectively. Eqs. (14) and (15) can be evaluated more easily and quickly than (5) and (6).

2.3. Special cases

2.3.1. Chan et al.'s transient-state solution [5]

Chan et al. [5] considered the problem with constant head boundaries at the wedges, and the hydraulic heads are zero on the boundaries. Thus, the boundary and initial conditions can be written as:

$$h(r,\theta,t) = p(r) = 0, \qquad \theta = 0, \quad 0 \leqslant r \leqslant \infty \quad (23)$$

$$h(r,\theta,t) = q(r) = 0, \qquad \theta = \phi, \quad 0 \leqslant r \leqslant \infty \quad (24)$$

$$h(r,\theta,0) = 0, \qquad 0 \leqslant \theta \leqslant \phi, \quad 0 \leqslant r \leqslant \infty \quad (25)$$

They solved (1) and (23)–(25) using the finite sine transform and Hankel transform, and the result was:

$$h(r,\theta,t) = \frac{2}{\phi}\frac{Q}{T}\sum_{n=1}^{\infty}\sin(\mu_n\theta)\sin(\mu_n\theta_0)(\Omega_1+\Omega_2) \quad (26)$$

Without accounting for the variety of topographic and hydrogeological boundary, the second, third and fourth term on the RHS of (5) become zero, and (5) reduces to (26). Thus, Chan et al.'s transient-state solution [5] can be considered as a special case of our solution (5). In addition, our transient-state solution of (14) becomes

$$h(r,\theta,t) = \frac{2}{\phi}\sum_{n=1}^{\infty}\sin(\mu_n\theta)\left[\frac{Q}{T}\sin(\mu_n\theta_0)\Omega_1\right] + \frac{Q}{4\pi T}(\log\gamma_1 - \log\gamma_2) \quad (27)$$

when neglecting the varying topographic and hydrogeological boundary. The integration of (8) is not straightforward to evaluate; on the other hand, the second term on the right-hand side of (27) is very easy to calculate. Therefore, our solution (27) is superior to Chan et al.'s transient-state solution in terms of numerical evaluation.

2.3.2. Chan et al.'s steady-state solution [5]

Based on (1) and (23)–(25), Chan et al. [5] further utilized the Mellin transform to obtain the steady-state hydraulic head solution as

$$h(r,\theta) = \frac{Q}{4\pi T}(\log\gamma_1 - \log\gamma_2) \quad (28)$$

Similarly, (28) was derived without accounting for the varying topographic and hydrogeological boundary. Eq. (15) can be simplified to (28) by setting the second, third and fourth term on the RHS of (15) to be zero. Thus, Chan et al.'s steady-state solution [5] can be also considered as a special case of our steady-state solution (15).

2.3.3. Problem with an impervious boundary condition

The problem with an impervious boundary at the lower wedge is shown in Fig. 3. The solution can be obtained by replacing ϕ with 2ϕ, setting the topographic parameters at the lower wedge to be zero, and inserting a second pumping well at the point $(r_0, 2\phi - \theta_0)$ in (14) and (15). For the time dependent component in (14),

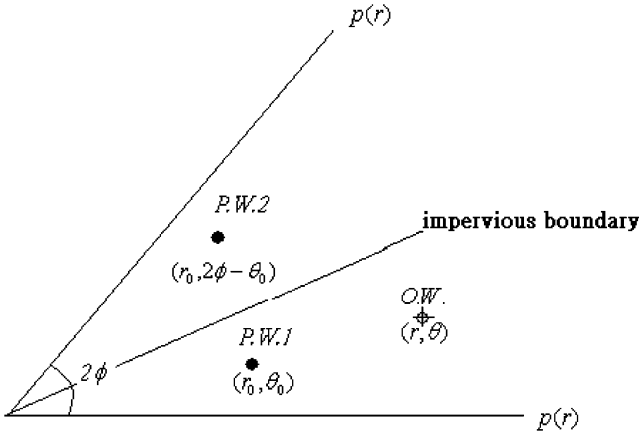

Fig. 3. The infinite wedge with impervious boundary at $\theta = \phi$.

$\mu_{n+\frac{1}{2}} = (2n+1)\pi/2\phi$ is used to replace $\mu_n = n\pi/\phi$. Thus, the transient-state and steady-state solutions for a wedge-shaped aquifer with an upper boundary of time-independent head and a lower impervious boundary can be respectively expressed as

$$h(r,\theta,t) = \frac{1}{\phi}\sum_{n=1}^{\infty}\sin\left(\mu_{n+\frac{1}{2}}\theta\right)\left[\frac{Q}{T}\sin\left(\mu_{n+\frac{1}{2}}\theta_0\right)\Omega_1\right] + \frac{Q}{4\pi T}(\log\gamma_1' - \log\gamma_2') + \frac{1}{\phi}\sum_{n=1}^{\infty}\sin\left(\mu_{n+\frac{1}{2}}\theta\right) \times \left[\frac{Q}{T}\sin\left(\mu_{n+\frac{1}{2}}(2\phi-\theta_0)\right)\Omega_1\right] + \frac{Q}{4\pi T}(\log\gamma_3 - \log\gamma_4) + \frac{c_1' r\cos(\phi-\theta)}{\cos\phi} + \varphi' a_1' \Lambda_1' + h_p \quad (29)$$

and

$$h(r,\theta) = \frac{Q}{4\pi T}(\log\gamma_1' - \log\gamma_2') + \frac{Q}{4\pi T}(\log\gamma_3 - \log\gamma_4) + \frac{c_1' r\cos(\phi-\theta)}{\cos\phi} + \varphi' a_1' \Lambda_1' + h_p \quad (30)$$

where

$$\Lambda_1' = \int_0^{\infty}\frac{(u^{(3\pi/\phi)-1} + r^{\pi/\phi}u^{\pi/2\phi})\sin(b_1' u)}{\psi_1}\,\mathrm{d}u \quad (31)$$

$$\varphi' = \frac{r^{\pi/2\phi}\sin\left(\frac{\pi}{2\phi}\theta\right)}{\phi} \quad (32)$$

$$\gamma_1' = 1 - 2\left(\frac{r}{r_0}\right)^{\pi/2\phi}\cos\frac{\pi(\theta+\theta_0)}{2\phi} + \left(\frac{r}{r_0}\right)^{\pi/\phi} \quad (33)$$

$$\gamma_2' = 1 - 2\left(\frac{r}{r_0}\right)^{\pi/2\phi}\cos\frac{\pi(\theta-\theta_0)}{2\phi} + \left(\frac{r}{r_0}\right)^{\pi/\phi} \quad (34)$$

$$\gamma_3 = 1 - 2\left(\frac{r}{r_0}\right)^{\pi/2\phi}\cos\frac{\pi(\theta+2\phi-\theta_0)}{2\phi} + \left(\frac{r}{r_0}\right)^{\pi/\phi} \quad (35)$$

and

$$\gamma_4 = 1 - 2\left(\frac{r}{r_0}\right)^{\pi/2\phi}\cos\frac{\pi(\theta-2\phi+\theta_0)}{2\phi} + \left(\frac{r}{r_0}\right)^{\pi/\phi} \quad (36)$$

If $r > r_0$, the solution can be obtained by interchanging r and r_0 in (33)–(36).

2.4. New mathematical formulas for Bessel functions

It is worth noting that three new mathematical formulas for Bessel functions are established in Appendix B. Based on (B.1) and (B.6), the second term on the RHS of (5) can be written as

$$\sum_{n=1}^{\infty}\frac{1}{\phi}\sin(\mu_n\theta)\sin(\mu_n\theta_0)\int_0^{\infty}J_{\mu_n}(ur_0)J_{\mu_n}(ur)\frac{\mathrm{d}u}{u} = \frac{1}{8\pi}(\log\gamma_1 - \log\gamma_2) \quad (37)$$

Based on (B.2) and (B.9), the third term on the RHS of (5) can be expressed as

$$\sum_{n=1}^{\infty}\frac{2n\pi}{\phi^2}\sin(\mu_n\theta)\int_0^{\infty}\frac{J_{\mu_n}(ur)}{u}\int_0^{\infty}J_{\mu_n}(ur)\,\mathrm{d}r\,\mathrm{d}u = \frac{\sin(\phi-\theta)}{\sin\phi}r \quad (38)$$

Furthermore, based on (B.10), the fourth term on the RHS of (5) can be written as

$$\sum_{n=1}^{\infty}\frac{2n\pi}{\phi^2}\sin(\mu_n\theta)\int_0^{\infty}\frac{J_{\mu_n}(ur)}{u}\int_0^{\infty}\sin(b_1' r)\frac{J_{\mu_n}(ur)}{r}\,\mathrm{d}r\,\mathrm{d}u = \frac{r^{\pi/\phi}\sin\left(\frac{\pi}{\phi}\theta\right)}{\phi}\int_0^{\infty}\frac{u^{(\pi/\phi)-1}\sin(b_1' u)}{u^{2\pi/\phi} - 2r^{\pi/\phi}u^{\pi/\phi}\cos\left(\frac{\pi}{\phi}\theta\right) + r^{2\pi/\phi}}\,\mathrm{d}u \quad (39)$$

Eqs. (37)–(39) consist of an infinite series containing an infinite integral of Bessel functions (or double infinite integral of Bessel functions). The LHS terms of (37)–(39) may be obtained when using the Hankel transform to solve the parabolic equations and are generally difficult to evaluate due to the oscillatory nature and slow convergence of the Bessel functions. Thus, these three formulas, (37)–(39), may serve as useful mathematical tools to simplify the results obtained from the Hankel transform. In addition, (37) can be considered as a formula which proves the equality between the steady-state solution derived via Hankel transform and the one derived via Mellin transform given in Chan et al. [5].

3. Numerical evaluations

The improper integrals of (14) and (15) may be difficult to directly evaluate due to the slow convergence of the Bessel functions and trigonometric functions. However, these integrals may be transformed as a sum of infinite series and each term of the series is obtained by integrating the area under the integrand and between two consecutive roots along a horizontal axis. Fig. 4 shows plots of the integrand of Ω_1 (Eq. (7)) in (14) versus u for $T = 1000\ \mathrm{m^2/day}$, $S = 0.0001$, $r_0 = 100$ m, $r = 200$ m, and $\mu_n = 3$, 6, or 12, and shows the oscillatory nature of the integrand. This figure displays that the integrand will converge slowly for the large μ_n. In addition, the value of the integrand of Ω_1 approaches zero for large u. Fig. 5 shows plots of the integrand of Λ_1 versus u for $b_1' = 0.0042$, $\theta = 10°$, $\phi = 60°$ and $r = 1000$, 5000, or 7500 m. For a fixed value of b_1', the integrand of Λ_1 not only has the same roots for various values of r, but also displays decreasing amplitudes of the oscillation with increasing r. Since the components of the integrand of Λ_2 are similar to those of Λ_1, the plot the integrand of Λ_2 is also similar to that of Λ_1. From

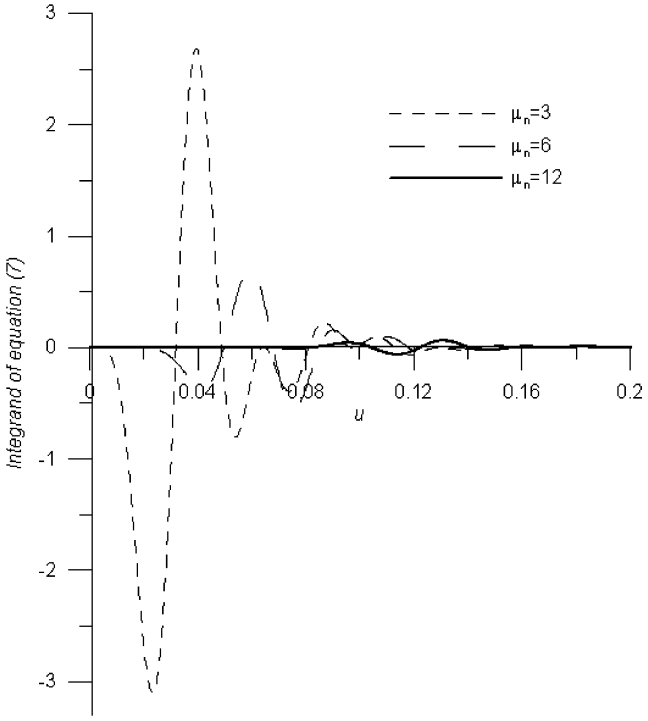

Fig. 4. The integrand of Eq. (7) versus the argument u.

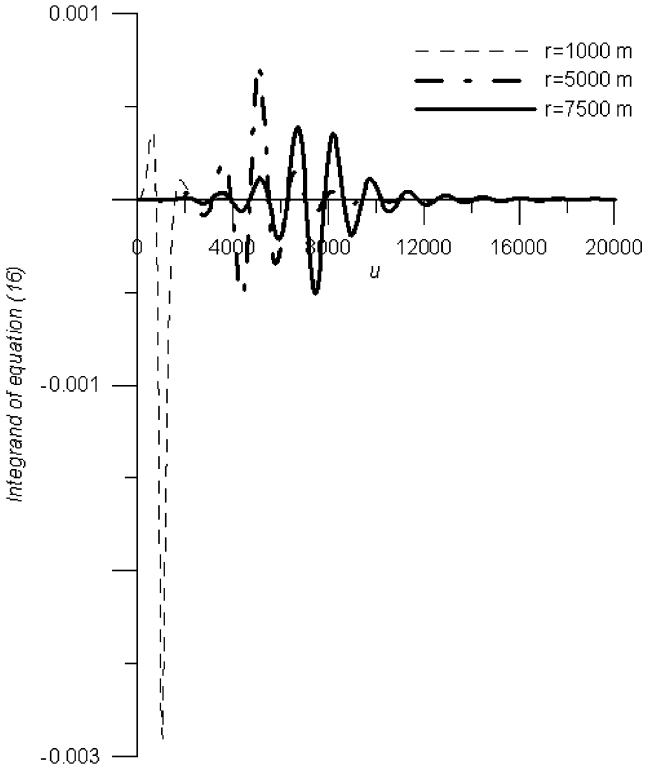

Fig. 5. The integrand of Eq. (16) versus the argument u.

the curves shown in Fig. 4, one can find the roots of the integrand of Ω_1 by a root search scheme. These curves demonstrate persistent oscillations over many cycles, and the amplitude of oscillation decreases with the horizontal axis. In addition, these formulas are essentially composed of infinite series and may converge slowly. Thus, the Gaussian quadrature is utilized to evaluate the integral, and the Shanks method [12] is employed to accelerate the convergence when evaluating the series. The root search scheme employs the Newton's method along with suggested increments to find the consecutive roots of the integrand along the u-axis. For each area under the integrand and between two consecutive roots, the Gaussian quadrature [3,6] is chosen to perform numerical integrations. Finally, Shanks' method [12] is applied to accelerate the convergence when evaluating the related Bessel functions, trigonometric functions and the infinite series in these solutions.

Notably, (14) has an integral composing of $J_v(u)$. The formulas used to approximate the functions are given in Abramowitz and Stegun [1] and listed below:

$$J_v(u) = \left(\frac{1}{2}u\right)^v \sum_{k=0}^{\infty} \frac{\left(-\frac{1}{4}u^2\right)^k}{k!\Gamma(v+k+1)} \tag{40}$$

This series converges for all u and yet is not computationally efficient when $u \gg 1$. The Bessel functions satisfy the following recurrence relation:

$$J_{n+1}(u) = \frac{2n}{u}J_n(u) - J_{n-1}(u) \tag{41}$$

However, (41) is unstable in the direction of increasing n. Indeed, high-order Bessel functions cannot be generated by forward recurrence using (41) [10]. A practical strategy for computing the Bessel functions is divided into two tasks: first, compute J_0 and J_1, and second, use the recurrence relations stably to find the other J's. The argument u in these formulas composed of Bessel functions may be divided into two ranges, $[0,8]$ and $(8,\infty)$ for $J_0(u)$ and $J_1(u)$ for better accuracy. For $0 \leqslant u \leqslant 8$, $J_0(u)$ and $J_1(u)$ are approximated by rational functions in u. For $8 < u < \infty$, the following approximation forms are used for $n = 0$ and 1

$$J_0(u) = \sqrt{\frac{2}{\pi u}}\left[\cos\left(u-\frac{\pi}{4}\right)\left[\sum_{k=0}^{\infty}(-1)^k\frac{(0,2k)}{(2z)^{2k}}\right] - \sin\left(u-\frac{\pi}{4}\right)\left[\sum_{k=0}^{\infty}(-1)^k\frac{(0,2k+1)}{(2z)^{2k+1}}\right]\right] \tag{42}$$

and

$$J_1(u) = \sqrt{\frac{2}{\pi u}}\left[\cos\left(u-\frac{3\pi}{4}\right)\left[\sum_{k=0}^{\infty}(-1)^k\frac{(1,2k)}{(2z)^{2k}}\right] - \sin\left(u-\frac{3\pi}{4}\right)\left[\sum_{k=0}^{\infty}(-1)^k\frac{(1,2k+1)}{(2z)^{2k+1}}\right]\right] \tag{43}$$

where

$$(\upsilon, m) = \frac{\Gamma\left(\upsilon+m+\frac{1}{2}\right)}{m!\Gamma\left(\upsilon-m+\frac{1}{2}\right)} \tag{44}$$

and $\Gamma(m)$ is the Gamma function [10]. As for $J_n(u)$, the recurrence of (41) can be started upward on n from J_0 and J_1; however, it remains stable only for $n < u$. The Bessel functions for $u < n$ can be obtained using Miller's algorithm [10, p. 175].

Because the oscillation of the integrand of Ω_1 is due to the terms of Bessel function $J_v(u)$, one may find the roots of the integrand of Ω_1 form the roots of $J_v(u)$; and the roots of $J_v(u)$ may be found by a conjunctive use of the following suggested increments for locating the roots and Newton's method for iteratively converging to the root. The asymptotic expansion of the large positive ith root of $J_v(u)$ for a given v is

$$j_{v,i} = \beta - (4v^2 - 1)/8\beta - [4(4v^2 - 1)(28v^2 - 31)]/3(8\beta)^3 \quad (45)$$

with $\beta = (\pi/4)(2v + 4i - 1)$. The increments Δ_1 from the origin to the first root approximated by $j_{v,1}$. The remaining increments Δ_i are chosen as $j_{v,i-1} - j_{v,i-2}$, and the remaining roots are approximately equal to $j_{v,i} = j_{v,i-1} + \Delta_i$, where $i = 2, 3, \ldots$ The roots of $J_v(u)$ using Newton's method and the suggested increments have the accuracy of seven significant.

4. Results and discussion

For the numerical evaluations, Table 1 lists the approximate roots and the values of Bessel functions using (45) and Newton's method. It shows that the value of Bessel functions for the approximate roots approach zero, which means the approximate roots are fairly close to the real roots based on the suggested increments when using Newton's method to determine roots. The roots of $J_v(u)$ have the accuracy of seven significant, which ensures that the solutions are evaluated with high accuracy. Several cases are considered in this paper. Table 2 lists the wedge angle and the topographical parameters for cases (a)–(c) as the ancient alluvial fans with various boundaries. Assume that there is a single pumping well located at $r_0 = 1000$ m and $\theta_0 = 30°$ in these alluvial fans with a pumping rate 30,000 m^3/day for 2 days. These cases can be regarded as the applications of the analytical solutions. The configurations of the hydraulic head distribution for cases (a)–(c) are also shown in Fig. 6(a)–(c) respectively. Different angles of the wedge-shaped aquifer and topographic parameters of the rechargeable boundaries cause significantly different configurations of the hydraulic head distribution within the wedge-shaped aquifer.

Fig. 7 demonstrates the transient-state drawdown of the wedge-shaped aquifer for a pumping well located at $(1000, 30°)$ with the pumping rate 30,000 m^3/day and two observation wells located at $(900, 30°)$ and $(1200, 45°)$ respectively with the boundary of time-independent head. These curves indicate that the drawdown increases with time, and the system tends to reach

Table 1
Approximated roots and values of $J_v(u)$ for $v = 3$, 6 and 12

i	$v = 3$		$v = 6$		$v = 12$	
	Approximated roots ($j_{v,i}$)	$J_v(j_{v,i})$	Approximated roots ($j_{v,i}$)	$J_v(j_{v,i})$	Approximated roots ($j_{v,i}$)	$J_v(j_{v,i})$
1	6.38016	5.42×10^{-8}	9.93611	-1.84×10^{-8}	0.00	0.00
2	9.76102	8.36×10^{-8}	13.58929	9.07×10^{-8}	20.78991	1.06×10^{-7}
3	13.015	2.70×10^{-8}	17.00382	-1.24×10^{-7}	24.49488	1.54×10^{-7}
4	16.22347	1.34×10^{-7}	20.32079	9.52×10^{-8}	28.02671	8.14×10^{-8}
5	19.40942	-3.38×10^{-7}	23.58608	1.12×10^{-7}	31.45996	-1.73×10^{-7}
6	22.58273	1.09×10^{-7}	26.82015	7.27×10^{-8}	34.82999	1.06×10^{-7}
7	25.74817	9.72×10^{-8}	30.03372	5.60×10^{-8}	38.15638	5.26×10^{-8}
8	28.90835	3.02×10^{-7}	33.23304	-5.93×10^{-8}	41.45109	5.25×10^{-8}
9	32.06485	2.30×10^{-7}	36.42202	-2.38×10^{-7}	44.72194	-4.01×10^{-8}
10	35.21867	1.44×10^{-8}	39.60324	-9.42×10^{-8}	47.97429	2.11×10^{-8}
10^2	314.9308	-3.55×10^{-7}	319.6011	-4.89×10^{-7}	328.8633	1.35×10^{-7}
10^3	3142.377	-6.09×10^{-7}	3147.085	6.59×10^{-7}	3156.492	2.66×10^{-7}

Table 2
The wedge angle and the topographical parameters of the boundary of time-independent head for various cases

Case	Wedge angle, ϕ	Topographical parameters for lower and upper boundaries			
		a_1[a]/a_2[a]	b_1[b]/b_2[b]	α_1[c]/α_2[c]	h_1[d]/h_2[d]
a	60°	10/10	0.004/0.004	1.14°/1.14°	100/100
b	120°	10/15	0.004/0.008	1.14°/0.57°	100/85
c	47°	10/15	0.004/0.008	1.14°/0.57°	100/85

[a] a represents the amplitude of the sine curve for the boundary.
[b] b represents the frequency for the boundary.
[c] α represents the average slope for the boundary.
[d] h represents the depth for the boundary at the origin of the wedge-shaped aquifer.

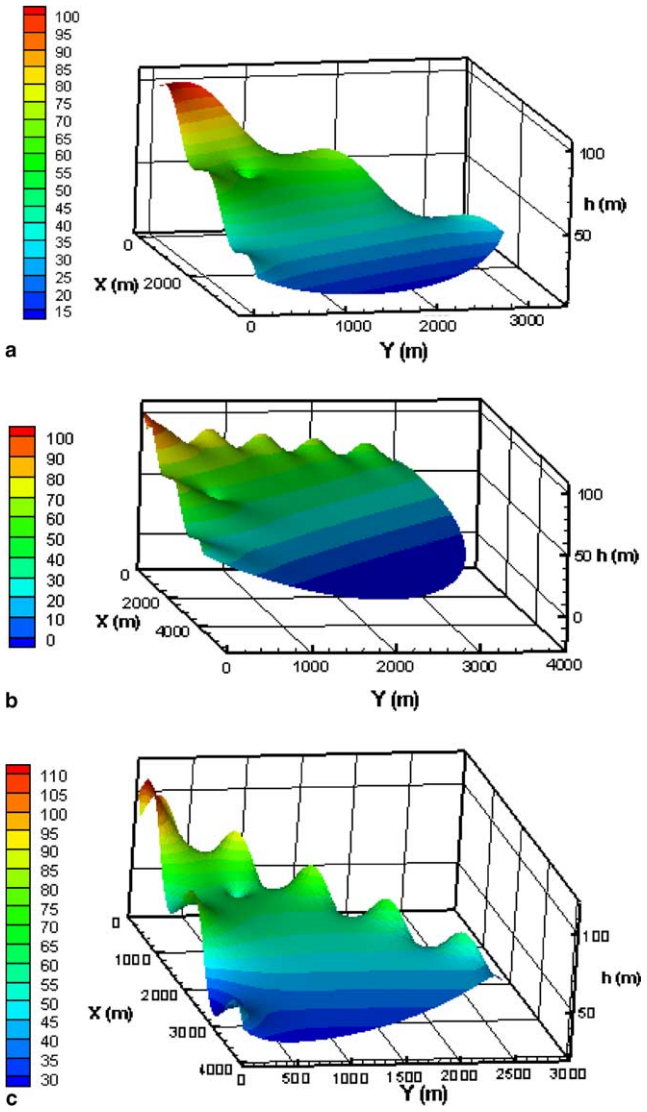

Fig. 6. Hydraulic head distributions for cases (a)–(c).

steady-state after 100 h at (900, 30°) and after 150 h at (1200, 45°).

5. Conclusions

A mathematical model for a wedge-shaped aquifer with various topographic and hydrogeological boundary conditions is presented. These solutions are derived via the Fourier finite sine transform and the Hankel transform. These solutions are further simplified to concise forms for easy computing. This paper extends the boundary conditions of the problem investigated by Chan et al. [5] to a more general case. In addition, this paper also improves the results of Chan et al. and simplifies some of their expressions to allow for easier numerical evaluation. New formulas (37)–(39) relate the steady-state solution derived via the Hankel transform to the solution derived via the Mellin transform in Chan et al. [5]. The transient-state solution consists of an infinite series containing an infinite integral of Bessel functions and the steady-state solution also consists of an infinite integral of trigonometric functions. Therefore, a unified numerical method, including the use of Newton's method, Gaussian quadrature, and Shanks' method, is proposed for efficiently evaluating the analytical solutions. This numerical method utilizes Newton's method along with suggested increments to find the consecutive roots of the integrand along the horizontal axis. For each roots, the Gaussian quadrature is chosen to perform the numerical integrations. Finally, Shanks' method is applied to accelerate the convergence when evaluating the integrals of Bessel functions and trigonometric functions and the infinite series.

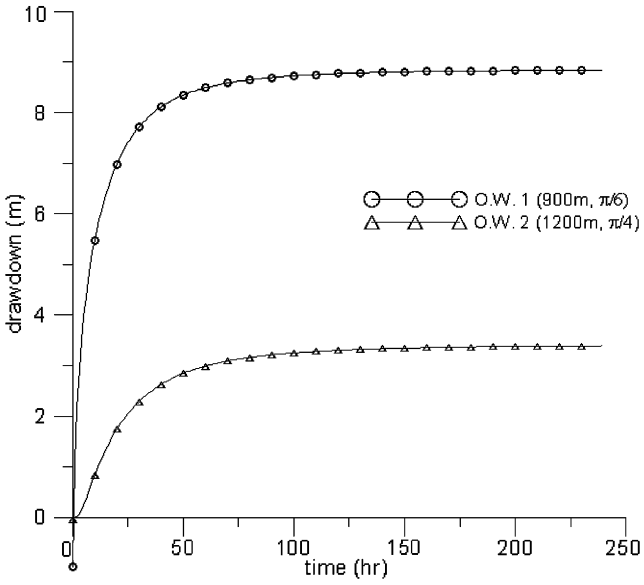

Fig. 7. The transient state drawdown for the wedge-shaped aquifer with rechargeable boundaries.

These newly derived solutions may have advantages of serving the following purposes: (1) to describe the groundwater flow in a wedge-shaped aquifer under various topographic and hydrogeological boundary conditions, (2) to predict drawdown for any wedge angle of the aquifer that the traditional method of image is not applicable, (3) to evaluate the sensitivity of the parameters in the mathematical model, and (4) to identify the hydraulic parameters when coupling with an optimization approach in aquifer data analysis.

Acknowledgments

Research leading to this paper has been partially supported by the grant from Taiwan National Science Council under the contract number NSC 93-2218-E-

009-056. The authors would like to thank three anonymous reviewers for their valuable and constructive comments.

Appendix A. Derivations of (5) and (6)

Taking the finite sine transform of (1), (3) and (4), the problem becomes:

$$T\left\{\frac{\partial^2\bar{h}}{\partial r^2}+\frac{1}{r}\frac{\partial\bar{h}}{\partial r}-\frac{\mu_n^2}{r^2}\bar{h}+\frac{\mu_n}{r^2}[p(r)-(-1)^n q(r)]\right\}-S\frac{\partial\bar{h}}{\partial t}=-\frac{Q}{r}\delta(r-r_0)\sin(\mu_n\theta_0) \tag{A.1}$$

where $\mu_n=n\pi/\phi$ with $n=1,2,3,\ldots$ Next, for eliminating the r coordinate, the Hankel transform $\hat{f}(u)=\int_0^\infty rf(r)J_v(ur)\,\mathrm{d}r$ is used to obtain

$$-u^2\hat{\bar{h}}-\frac{S}{T}\frac{\partial\hat{\bar{h}}}{\partial t}=-\frac{Q}{T}J_{\mu_n}(ur_0)\sin(\mu_n\theta_0)-\mu_n\int_0^\infty[p(r)-(-1)^n q(r)]J_{\mu_n}(ur)\frac{\mathrm{d}r}{r} \tag{A.2}$$

where $J_{\mu_n}(\cdot)$ is the Bessel function of the first kind of order μ_n. When $t=0$, the term $\partial\hat{\bar{h}}/\partial t$ is omitted and the pumping rate Q is set to be zero; thus, the initial condition can be specified as:

$$\hat{\bar{h}}(u,n,0)=\frac{\mu_n}{u^2}\int_0^\infty[p(r)-(-1)^n q(r)]J_{\mu_n}(ur)\frac{\mathrm{d}r}{r} \tag{A.3}$$

Consequently, (A.2) can be solved with (A.3) as

$$\hat{\bar{h}}(u,n,t)=\frac{Q}{T}\frac{1}{u^2}J_{\mu_n}(ur_0)\sin(\mu_n\theta_0)[1-\exp(-u^2Tt/S)]+\frac{\mu_n}{u^2}\left[\int_0^\infty p(r)J_{\mu_n}(ur)\frac{\mathrm{d}r}{r}-(-1)^n\int_0^\infty q(r)J_{\mu_n}(ur)\frac{\mathrm{d}r}{r}\right] \tag{A.4}$$

Carrying out the inverse finite sine transform and inverse Hankel transform $f(r)=\int_0^\infty u\hat{f}(u)J_v(ur)\,\mathrm{d}u$ to (A.4), the hydraulic head solution for transient state can be expressed as (5) with (7)–(13). The steady-state solution can be solved by omitting $\partial\bar{\bar{h}}/\partial t$ term on the left-hand side of (A.2) and the result is expressed as (6). Actually (6) reduces to (5) when t approaches infinity.

Appendix B. Simplification of (5) and (6)

Since (5) contains the double integrals of Bessel functions, the evaluation for this equation is not an easy task for desired accuracy. Thus, the equation should be simplified to a more concise form for ease of computing. The integrations of (8) can be derived based on formula (72) of McLachlan [9] as

$$\Omega_2=\begin{cases}\frac{1}{2\mu_n}\left(\frac{r}{r_0}\right)^{\mu_n}, & r_0>r\\ \frac{1}{2\mu_n}\left(\frac{r_0}{r}\right)^{\mu_n}, & r>r_0\end{cases} \tag{B.1}$$

Likewise, the integrand of (9) and (12) can be obtained based on the formula (6.561-14) of Jeffrey et al. [7, p. 684] as

$$\Omega_3=\frac{r}{\mu_n^2-1} \tag{B.2}$$

and

$$\Omega_6=\frac{1}{\mu_n^2} \tag{B.3}$$

Therefore, (5) and (6) can be simplified by substituting (B.1), (B.2) and (B.3) into (8), (9) and (12) as

$$h(r,\theta,t)=\frac{2}{\phi}\sum_{n=1}^\infty\sin(\mu_n\theta)\left[\frac{Q}{T}\sin(\mu_n\theta_0)\left(\Omega_1+\frac{1}{2\mu_n}\left(\frac{r}{r_0}\right)^{\mu_n}\right)+\frac{\mu_n r}{\mu_n^2-1}(c_1'-(-1)^n c_2')+\mu_n(a_1'\Omega_4-(-1)^n a_2'\Omega_5)+\frac{1}{\mu_n}(h_p-(-1)^n h_q)\right] \tag{B.4}$$

and

$$h(r,\theta)=\frac{2}{\phi}\sum_{n=1}^\infty\sin(\mu_n\theta)\left[\frac{Q}{T}\sin(\mu_n\theta_0)\frac{1}{2\mu_n}\left(\frac{r}{r_0}\right)^{\mu_n}+\frac{\mu_n r}{\mu_n^2-1}(c_1'-(-1)^n c_2')+\mu_n(a_1'\Omega_4-(-1)^n a_2'\Omega_5)+\frac{1}{\mu_n}(h_p-(-1)^n h_q)\right] \tag{B.5}$$

By evaluating the sum, the first term on the RHS of (B.5) can be derived based on the formula (1.448-2) of Jeffrey et al. [7] as

$$\frac{2Q}{\phi T}\sum_{n=1}^\infty\sin(\mu_n\theta)\sin(\mu_n\theta_0)\frac{1}{2\mu_n}\left(\frac{r}{r_0}\right)^{\mu_n}=\frac{Q}{2\pi T}\sum_{n=0}^\infty\left[\cos\left(\frac{n\pi}{\phi}(\theta-\theta_0)\right)-\cos\left(\frac{n\pi}{\phi}(\theta-\theta_0)\right)\right]\frac{1}{n}\left(\frac{r}{r_0}\right)^{n\pi/\phi}=\frac{Q}{4\pi T}(\log\gamma_1-\log\gamma_2) \tag{B.6}$$

with (21) and (22).

And the second and fourth terms on the RHS of (B.5) can be derived based on the formulas (1.445-5) and (1.445-7) of Jeffrey et al. [7] as

$$\frac{2}{\phi}\sum_{n=1}^\infty\sin(\mu_n\theta)\frac{\mu_n r}{\mu_n^2-1}(c_1'-(-1)^n c_2')=\sum_{n=1}^\infty\sin\left(\frac{n\pi\theta}{\phi}\right)\frac{2n}{\pi}(c_1'-(-1)^n c_2')\frac{r}{n^2-\left(\frac{\phi}{\pi}\right)^2}=c_1'\frac{\sin(\phi-\theta)}{\sin\phi}r+c_2'\frac{\sin\theta}{\sin\phi}r \tag{B.7}$$

and

$$\frac{2}{\phi}\sum_{n=1}^{\infty}\sin(\mu_n\theta)\frac{1}{\mu_n}(h_p-(-1)^n h_q) = \frac{2h_p}{\pi}\sum_{n=1}^{\infty}\frac{\sin\left(\frac{n\pi\theta}{\phi}\right)}{n}-\frac{2h_q}{\pi}\sum_{n=1}^{\infty}(-1)^n\frac{\sin\left(\frac{n\pi\theta}{\phi}\right)}{n} = h_p+\frac{\theta}{\phi}(h_q-h_p) \tag{B.8}$$

The third term of (B.5) can be simplified by the Parseval's relation of Hankel transform [2], i.e.,

$$\int_0^\infty \hat{f}(u)\hat{g}(u)u\,\mathrm{d}u = \int_0^\infty u\hat{f}(u)\,\mathrm{d}u\int_0^\infty g(r)J_v(ur)r\,\mathrm{d}r = \int_0^\infty g(r)r\,\mathrm{d}r\int_0^\infty \hat{f}(u)J_v(ur)u\,\mathrm{d}u = \int_0^\infty f(r)g(r)r\,\mathrm{d}r \tag{B.9}$$

and the result can be obtained based on the formula (1.447-1) of Jeffrey et al. [7] as:

$$\frac{2}{\phi}\sum_{n=1}^{\infty}\sin(\mu_n\theta)\mu_n(a_1'\Omega_4-(-1)^n a_2'\Omega_5) = \varphi[a_1'\Lambda_1+a_2'\Lambda_2] \tag{B.10}$$

with (16)–(20).

By rearranging (B.6), (B.7), (B.8) and (B.10), the transient-state solution (5), can be written in a more concise form as (14). Notice that the first term on the RHS of (14) is the only term dependent on time in the equation. This term will reduce to zero when time approaches infinity. Thus, the steady-state solution for the hydraulic head within a wedge-shaped aquifer becomes as (15).

References

[1] Abramowitz M, Stegun IA. Handbook of mathematical functions with formulas, graphs and mathematical tables. Washington, DC: National Bureau of Standards, Dover; 1964.

[2] Adrews LC, Shivamoggi BK. Integral transforms for engineers. USA: SPIE Optical Engineering Press; 1999.

[3] Burden RL, Faires JD. Numerical analysis. Boston: PWS-KENT; 1989.

[4] Chan YK, Mullineux N, Reed JR. Analytical solutions for drawdowns in rectangular artesian aquifers. J Hydrol 1976;31:151–60.

[5] Chan YK, Mullineux N, Reed JR, Wells GG. Analytic solutions for drawdowns in wedge-shaped artesian aquifers. J Hydrol 1978;36:233–46.

[6] Gerald CF, Wheatley PO. Applied numerical analysis. Mass: Addison-Wesley; 1989.

[7] Jeffrey A, Ryzhik I, Gradshteyn I, Yu G, Tseytlin M. Tables of integrals, series, and products. New York: Academic Press; 1980.

[8] Kuo MCT, Wang WL, Lin DS, Chiang CJ. An image-well method for predicting drawdown distribution in aquifers with irregularly shaped boundaries. Ground Water 1994;32(5):794–804.

[9] McLachlan NW. Bessel functions for engineers. Great Britain: Oxford University Press; 1955.

[10] Press WH, Flannery BP, Teukolsky SA, Vetterling WT. Numerical recipes. London: Cambridge University Press; 1986.

[11] Schwartz FW, Zhang H. Fundamentals of ground water. New York: John Wiley & Sons Inc.; 2003.

[12] Shanks D. Non-linear transformations of divergent and slowly convergent sequence. J Math Phys 1955;34:1–42.

[13] Theis CV. The relation between the lowering of the piezometric surface and the rate and duration of discharge of a well using ground-water storage. Eos Trans AGU 1935;16:519–24.

[14] Toth J. A theoretical analysis of groundwater flow in small drainage basins. J Geophys Res 1963;68(16):4795–813.